BMC Microbiology

RESEARCH Open Access

Non-alcoholic fatty liver disease enhances the beneficial effect of renal denervation on gut microbiota aberrations in rats with heart failure

Fuyan Chen[1†], Zhiqin Guo[2†], Yufeng Chen[3], Shun Li[2] and Pingan Chen[1*]

Abstract

Background Renal denervation (RDN) contributes to improving cardiac function by ameliorating aberrations of the gut microbiota, and non-alcoholic fatty liver disease (NAFLD) is associated with gut microbiota dysbiosis and is critically involved in the development of heart failure (HF). It is unclear whether the beneficial effect of RDN on gut microbiota in HF can be affected by NAFLD and whether this effect changes with the severity of NAFLD.

Methods HF Sprague Dawley rats induced by transverse aortic constriction were fed a high-fat-fructose diet and underwent RDN, and sequencing of 16S rRNA gene in fecal samples was detected.

Results The dissimilarity coefficients and sample distances of the intestinal microbiome were elevated in HF rats with NAFLD. After RDN, HF rats with NAFLD had fewer bacteria harmful to cardiac function, such as *Alphaproteobacteria*, *Bacteroidota* and *Prevotella-9*, and more bacteria beneficial to HF, such as *Monoglobaceae, Proteobacteria* and *Monoglobales,* than HF rats without NAFLD (all $p < 0.05$). This tendency also existed but was much less significant when compared between HF rats with non-alcoholic steatohepatitis (NASH) and without NAFLD. Predictive functional profiling of microbial communities revealed that after RDN, the abundance of membrane transport, environmental and genetic information processing was significantly higher, and glycan biosynthesis and metabolism was significantly lower in HF rats with NAFLD than in those without NAFLD.

Conclusion NAFLD could further enhance the beneficial role of RDN in mitigating gut microbiota aberrations in HF rats by increasing beneficial bacteria and decreasing bacteria harmful to cardiac function, but this effect was not apparent in NASH rats.

Keywords Heart failure, Renal denervation, Gut microbiota, NAFLD

Introduction

Heart failure (HF) is the end stage of various heart diseases [1], and a growing array of studies shows that abnormalities in the gut microbiota and gut dysfunction are important factors in the development of heart failure [2, 3]. Renal denervation (RDN) is a potential approache for HF treatment by downregulating sympathetic nerve activity [4]. Furthermore, inhibiting the renin-angiotensin system [5], restoring neuronal nitric oxide synthase [6] and balancing the gut microbiota [7] are other important mechanisms by which RDN improves cardiac

†Fuyan Chen and Zhiqin Guo contributed equally to this work.

*Correspondence:
Pingan Chen
cpadejxyx@gzhmu.edu.cn
[1] Department of Cardiology, the Second Affiliated Hospital, School of Medicine, South China University of Technology, 1 Panfu Road, Guangzhou, Guangdong 510182, China
[2] Department of Cardiology, Guangzhou First People's Hospital, Guangzhou, China
[3] Department of Cardiology, Maoming People's Hospital, Maoming, China

function in addition to modulating sympathetic nerve activity. Our previous study also showed that RDN could ameliorate aberrations of the gut microbiota in HF rats [8]. Therefore, the alteration of the intestinal microbiota, especially by increasing beneficial bacteria and decreasing harmful bacteria to cardiac function, may also be one of the mechanisms by which RDN could improve HF [9].

Non-alcoholic fatty liver disease (NAFLD), which encompasses two pathological processes: namely, benign steatosis and steatohepatitis [10], is a major risk factor for HF and other cardiovascular diseases. NAFLD is associated with alterations in myocardial structure or function, which are thought to play an important role in the progression of HF [11, 12]. It has been shown that the development of NAFLD involves abnormal sympathetic nerve activity [13], and in NAFLD, the gut flora becomes dysbiotic, which can further contribute to NAFLD progression and the deterioration of HF [14]. These findings suggest that there is implied relationship between gut microbiota, NAFLD and RDN in HF. However, it is unclear whether the pattern and degree of the impact of RDN on ameliorating aberrations of the gut bacteria in HF can be altered in the presence of NAFLD.

This study was conducted to explore the changes in the gut microbiota in HF rats with NAFLD and to investigate the impaction of NAFLD, including different degrees of NAFLD, on the role of RDN in ameliorating aberrations of the gut microbiota in HF rats.

Methods

Animal grouping

Sprague-Dawley rats (weighing 70–100 g, 3 weeks old) were obtained from Guangdong Medical Experimental Animal Center (Foshan, China) and housed under a 12-h light-dark cycle with free access to food and water. After acclimatization for one week, the rats were assigned to six groups as follows: (1) the control group (Control, $n = 6$): regular diet, sham transverse aortic constriction (TAC) and sham RDN; (2) the NF. RDN group (HF+RDN, $n = 4$): regular diet, TAC and RDN; (3) the F. NRDN group (NAFLD+HF, $n = 5$): high-fat-fructose diet (60% kcal as fat, GD60, D12492, Guangdong Medical Experimental Animal Center, Foshan, China, with 30% w/v fructose in water, MB2500, Meilunbio, Jiayan Biotech Co., Ltd, Guangzhou, China) for 12 weeks, followed by TAC and sham RDN; (4) the F. RDN group (NAFLD+HF+RDN, $n = 4$): high-fat-fructose diet for 12 weeks, followed by TAC and RDN; (5) the FF. RDN group (NASH+HF+RDN, $n = 4$): high-fat-fructose diet for 16 weeks, followed by TAC and RDN; (6) the TF. RDN group (NAFLD+HF+RDN+UDCA, $n = 5$): high-fat-fructose diet for 12 weeks, followed by TAC, RDN and treatment with ursodeoxycholic acid (UDCA, 60 mg/kg/d, 6 weeks after RDN. Losan Pharma GmbH, Neuenburg, Germany) for 1 week (Supplemental Figure S1).

Construction of the heart failure model

TAC was performed as described in our previous study [9]. The rats (8 weeks old) were anesthetized with 2% pentobarbital sodium (30 mg/kg, intraperitoneally injected) and underwent TAC surgery by constricting the abdominal aorta. Sham TAC rats underwent the same surgical procedure described as above, but abdominal aortic narrowing was not performed.

Renal denervation

Eight weeks after TAC, the rats were subjected to RDN as previously described [9]. The rats were anesthetized with 2% pentobarbital sodium (30 mg/kg, intraperitoneally injected). After isolation from the surrounding tissue, the renal arteries were subsequently ablated with 10% phenol in absolute alcohol to ablate the sympathetic nerves. Saline, rather than phenol, was used to ablate the renal sympathetic nerves in sham RDN rats.

Establishment of the model of non-alcoholic fatty liver disease

At the fourth week of age, the rats were fed a high-fat diet (60% kcal as fat) with 30% w/v fructose in water for 12 weeks to develop NAFLD model, and for 16 weeks to develop non-alcoholic steatohepatitis (NASH) model as previously described [15–17].

Collection and extraction of fecal samples

At the 2nd week after UDCA or vehicle administration, the rats were sacrificed by an overdose of pentobarbital sodium (100 mg/kg). Formed feces in the distal colon were collected by opening abdomen. The fresh fecal samples were immediately removed into a liquid nitrogen tank, and then stored at −80°C until further processing. The above process was aseptic throughout. The CTAB/SDS method [8, 18, 19] was adopted to extract all of the genomic DNA from the samples, and the genomic DNA sample was diluted to 1 ng/μl using sterile water. Meanwhile, the liver and lung were obtained and weighted.

16S rRNA sequencing

16S rRNA sequencing was performed [8, 9, 18], and the V4 region of 16S rRNA gene was analyzed. The specific primers 515 F (5'-GTGCCAGCMGCCGCGGTAA-3') and 806R (5'-GGACTACHVGGGTWTCTAAT-3') with barcodes were adopted to amplify the 16S rRNA genes. After obtaining the target fragment, gel electrophoresis was carried out to detect the amplification effect and the size of the target fragment. Then the amplification product obtained was subjected to library construction,

and the library was sequenced using high-throughput sequencing technology. Then, the reads were quality controlled to get clean reads. All the effective reads of the samples were clustered into operational taxonomic units (OTUs) with 97% identity. All samples were normalized, and alpha and beta diversity were analyzed. Species annotation was performed based on the small subunit rRNA (SSU rRNA) database, and the community composition of each sample at different taxonomic levels was analyzed. Kyoto Encyclopedia of Genes and Genome (KEGG) pathway analyses were used to predict function based on bacterial 16S sequencing data by Tax4 Fun.

Echocardiography

As described previously [18], transthoracic echocardiography was performed using Vevo 2100 (Toronto, ON, Canada) imaging system with a 15 Mhz to 30 Mhz linear array transducer and two-dimensional M-mode. Rats were anesthetized with 3% isoflurane-oxygen and positioned supine. Anesthesia efficacy was confirmed by diminished limb muscle tone, and anesthesia was maintained with 2% isoflurane-oxygen. Parasternal short-axis and long-axis view were observed. The following parameters were measured and collected: left ventricular end-diastolic volume and diameter (LVVd and LVDd), left ventricular end-systolic volume and diameter (LVVs and LVDs), and mitral valve E and A velocity. Left ventricular ejection fraction (LVEF, %) were calculated using the equation respectively: LVEF = 100×(LVVd - LVVs)/LVVd. All echocardiographic measurements were performed blinded to grouping and validated by an independent investigator.

Hematoxylin eosin and Masson's staining

Paraffin embedded rat liver slices (4 μm) were deparaffinized in xylene and rehydrated with graded ethanol series. Slices were stained with hematoxylin and eosin or Masson's trichrome according to standard protocols. After air drying, observe the sections under an optical microscope to evaluate hepatic cell degeneration and the degree of fibrosis.

Oil red O staining

Rat liver tissues were embedded and sectioned into frozen slices (8 μm). Sections were rinsed with 60% isopropanol, stained with Oil Red O working solution for 10 minutes, and washed again with 60% isopropanol. Nuclei were counterstained with hematoxylin for 5 minutes. Sections were then examined under a light microscope to evaluate hepatocyte steatosis.

Statistical analysis

Alpha diversity was represented by Chao1 and Shannon indexes. Principal co-ordinates analysis (PCoA) based on the weighted or unweighted UniFrac distance, and non-metric multidimensional scaling (NMDS) were performed using R software to describe beta diversity. To determine the differences in microbial communities between groups, analysis of similarity (ANOSIM) and analysis of molecular variance (AMOVA) were carried out. The differences in individual taxonomy between groups were analyzed by Metastats (http://metastats.cbcb.umd.edu/). The statistically different biomarkers in the different groups were quantitatively analyzed by linear discriminant analysis effect size (LEfSe). Wilcoxon rank sum test analysis was used to test data that did not conform to a normal distribution between two groups. Welch's t-test analysis was used to test data with different variances between two groups and detect bacterial communities with significant differences between two groups more accurately. p values were two-sided and considered significant when $p < 0.05$. Statistical analysis was performed using SPSS software (SPSS version 20.0).

Results

The composition of the gut microbiota varied among the different groups

Compared with the control group, rats in the F.RDN (rats with NAFLD) and FF.RDN (rats with NASH) groups had higher body weight, and the body weight of rats in the FF.RDN group was greater than that in the F.RDN group (Supplemental Fig. S2 A). Furthermore, compared with the control group, rats in the FF.RDN group had higher liver index (liver weight/bodyweight × 100%) ($p<0.05$). The liver index of the F.RDN group was also higher than that of the control group, though the difference was not significant (Supplemental Fig. S2 B). As shown in Supplemental Figure S3, HE staining of liver showed that rats with NAFLD (including the F.NRDN, F.RDN, FF.RDN and TF.RDN groups) exhibited characteristic hepatocyte ballooning and disrupted hepatic cord architecture compared with the controls. Notably, the FF.RDN group (NASH rats) demonstrated marked steatohepatitis with lipid droplet accumulation. It is reported that steatohepatitis with lipid droplet accumulation is characterized by NASH [20].

In addition, Oil red O (lipid quantification) and Masson's staining (fibrosis assessment) revealed that lipid content (Supplemental Fig. S4 A-B) and collagen deposition (Supplemental Fig. S4 C-D) in the F.NRDN, F.RDN and FF.RDN groups were significantly increased than in the control group (all $p<0.05$). Supplemental Figure S4 also showed the mild attenuation of NAFLD pathology

in the TF.RDN group compared with the F.RDN and FF.RDN groups and aggravated steatosis (Supplemental Fig. S4 A-B) and fibrosis (Supplemental Fig. S4 C-D) in the FF.RDN group compared with the F.RDN group (all $p<0.05$).

Furthermore, echocardiography was performed to assess cardiac function in rats receiving transverse aortic constriction (TAC). Ultrasonic cardiogram showed that the F.NRDN group had lower LVEF, E/A ratio and larger LVDs and lung to body weight index compared with the Control group (both $p<0.05$). LVEF was increased in the NF.RDN and F.RDN groups compared with the F.NRDN group (both $p<0.05$). Left ventricular end-diastolic diameter were increased in the F.NRDN group compared with the Control group though the difference was not significant (Supplemental Fig. S4 E-I).

An average of 64491 sequences per sample was obtained, and these sequences were clustered into a total of 2407 OTUs at a 97% similarity threshold (Fig. 1A). Figure 1B showed the sequences were clustered into 372 OTUs in the NF. RDN group, 355 in the F. RDN group and184 in the FF. RDN group.

Alpha diversity analysis represented by Chao 1 (Fig. 1C) and Shannon (Fig. 1D) analysis indicated the significant differences in the abundance of the gut microbiota between the control, NF. RDN, F. NRDN, F. RDN and FF. RDN groups. Beta diversity revealed that the dissimilarity coefficients increased gradually with the development of NAFLD in HF rats. The weighted UniFrac distance was 0.121 in the TF. RDN group, 0.146 in the F. RDN group, and 0.420 in the FF. RDN group when compared with the NF. RDN group (Fig. 1E).

PCoA revealed that the respective distance between the control and NF. RDN, TF. RDN groups was shorter than that between the control and F. RDN, FF. RDN groups (Fig. 1F). NMDS statistics showed that the stress was 0.098 (weighted) and 0.092 (unweighted) (stress < 0.2 was used as an acceptable threshold), indicating that NMDS accurately reflected the degree of difference between samples (Fig. 1G). The samples distance of the FF. RDN group was far from the control, NF. RDN, F. NRDN, F. RDN and TF. RDN groups. The distance between the NF. RDN and F. RDN groups was greater than that between the NF. RDN and TF. RDN groups (Fig. 1F, G), suggesting that microbial diversity could be affected by the serious degree of NAFLD. The significance of differences was confirmed by the tests of ANOSIM (Table 1).

LEfSe analysis revealed that the NF. RDN group had a higher abundance of *Clostridia_UCG-014* and *Prevotella_9*, while the F. RDN group had more *Gammaproteobacteria* than the control group (Fig. 1H and I). The results revealed that there were differences in the composition of gut microbiota in the control, F. RDN, and NF. RDN groups.

Analysis of gut microbiota composition at the phylum level

The NF. RDN group showed a higher presence of *Cyanobacteria*. The FF. RDN group had increased levels of *Fusobacteriota*, *Proteobacteria*, *Actinobacteria* and *Patescibacteria*, and decreased levels of *Firmicutes* and *Bacteroidota*, indicating an imbalance in the bacterial structure. The TF. RDN group had more *Elusimicrobiota*, *Campylobacterota* and *Verrucomicrobiota* (Fig. 2A).

Top ten microbial communities showed that *Proteobacteria* existed mainly in the F. RDN (9%), FF. RDN (44%) and TF. RDN (2%) groups. The abundance of *Firmicutes* was increased significantly in the F. RDN (73%) and TF. RDN (72%) groups compared with the FF. RDN group (48%). The ratio of Firmicutes to *Bacteroidota* (F/B) was 3.18 in the TF. RDN group, and it was 5.21 in the F. RDN group, which was higher than that in the NF. RDN group (2.74) (Fig. 2B).

Wilcoxon rank sum test analysis showed that the F. RDN group had fewer *Bacteroidota* (Fig. 2C) and more *Proteobacteria* (Fig. 2D) than the NF. RDN group. Welch's t-test analysis showed the abundance of *Bacteroidota* was lower in the FF. RDN group than in the NF. RDN (Fig. 3C) and TF. RDN groups (Fig. 3E).

Analysis of the gut microbiota composition at the class level

The NF. RDN group had more *Alphaproteobacteria*. *Unidentified_Firmicutes* and *Deferribacteres* were the dominant bacteria in the F. NRDN group and *Negativicutes* was the dominant bacteria in the F. RDN group. The FF. RDN group had more *Fusobacteriia*,

(See figure on next page.)

Fig. 1 Alpha and beta diversity and differences in the gut microbiota among the different groups. **A** Rarefaction diversity of different samples based on observed species number. **B** Petal diagram of the six groups. **C** Alpha diversity for various groups based on Chao1 index and (**D**) Shannon index. **E** Dissimilarity coefficient of the beta diversity heatmap based on the weighted (upper value) and unweighted (lower value) UniFrac distances of groups. **F** PCoA based on the weighted and unweighted Unifrac distance. **G** NMDS analysis of bacterial population structure [stress = 0.098 (weighted) and 0.092 (unweighted)]. **H** The dominant species in the control (red), NF. RDN (blue) and F. RDN groups (green). **I** Taxonomic cladogram obtained from LEfSe. Taxa meeting a linear discriminant analysis significance threshold > 4 were shown (c: class level; f: family level; o: order level). The circle's diameter of each circle was proportional to the taxonomic abundance. RDN, renal denervation; PCoA, principal co-ordinates analysis; NMDS, nonmetric multidimensional scaling; LEfSe, linear discriminant analysis effect size

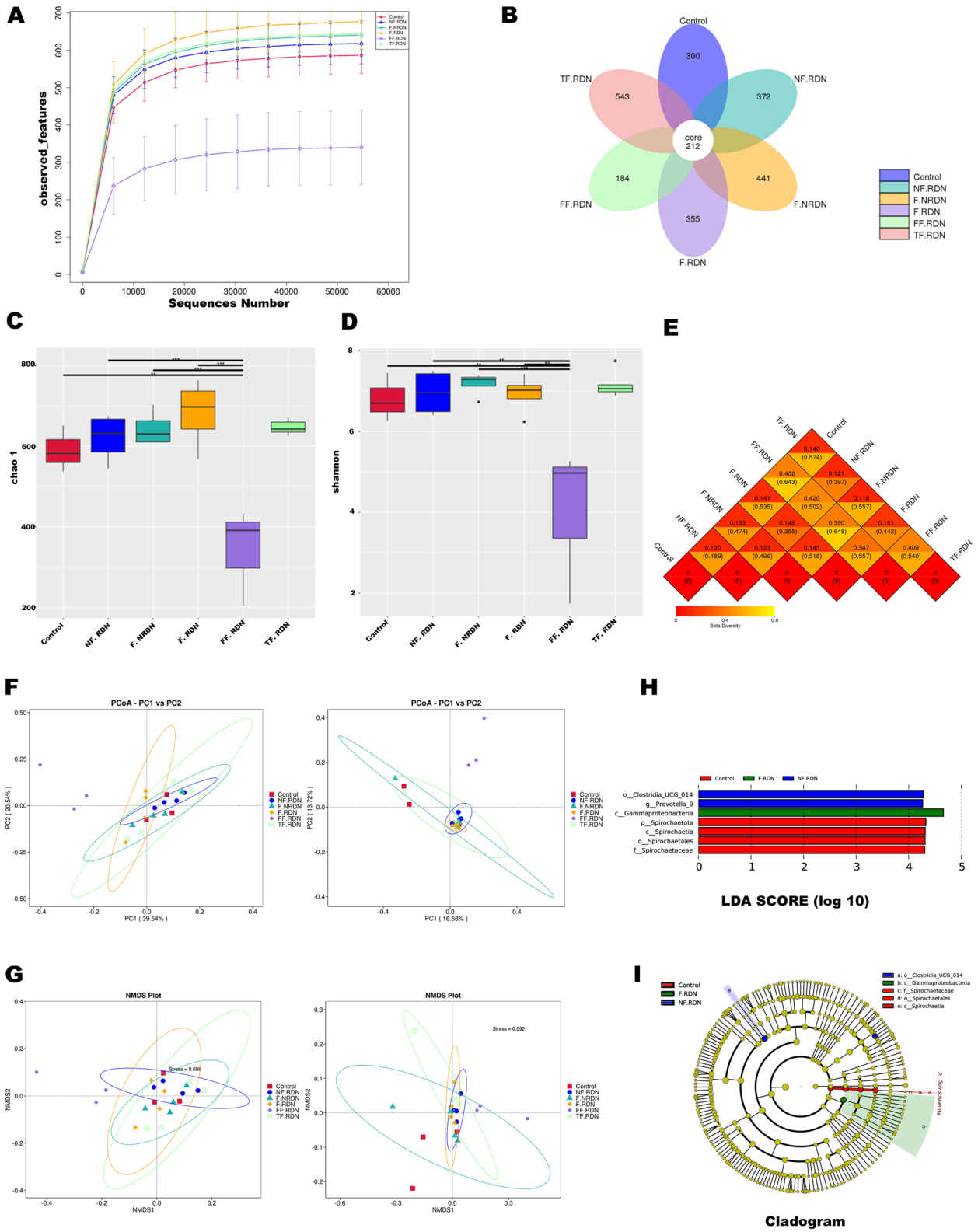

Fig. 1 (See legend on previous page.)

Table 1 Significance tests on community structures between groups with ANOSIM tests

Groups	ANOSIM	
	R	*P*
Control vs. NF.RDN	0.074	0.290
Control vs F.NRDN	−0.148	0.663
Control vs F.RDN	0.296	0.096
Control vs FF.RDN	0.963	0.100
Control vs TF.RDN	0.641	**0.013**
NF.RDN vs F.NRDN	−0.156	0.797
NF.RDN vs F.RDN	0.187	0.194
NF.RDN vs FF.RDN	0.981	**0.034**
NF.RDN vs TF.RDN	0.213	0.150
F.NRDN vs F.RDN	0.208	0.154
F.NRDN vs FF.RDN	0.722	**0.026**
F.NRDN vs TF.RDN	0.206	0.119
F.RDN vs FF.RDN	0.796	**0.030**
F.RDN vs TF.RDN	0.419	**0.047**
FF.RDN vs TF.RDN	0.805	**0.015**

Bold values indicate statistical significance ($P < 0.05$). In the ANOSIM test, $R > 0$ indicated that the differences between the groups were larger than the differences within the groups. ANOSIM: analysis of similarity

Gammaproteobacteria and *Saccharimonadia*. while *Elusimicrobia* and *Campylobacteria* were dominant in the TF. RDN group (Fig. 2E).

The top ten microbial communities showed the proportion of *Bacteroidia* was 26% in the NF. RDN group, 14% in the F.RDN group, 2% in the FF. RDN group, and 23% in the TF. RDN group (Fig. 2F). The abundances of *Bacteroidia* (Fig. 2G) and *Alphaproteobacteria* (Fig. 2H) were lower in the F. RDN group than in the NF. RDN group.

Welch's t-test analysis showed that the abundance of *Alphaproteobacteria* was lower in the F. RDN group than in the NF. RDN group (Fig. 3B). The NF. RDN group had more *Alphaproteobacteria* and *Bacteroidia* compared with the FF. RDN group (Fig. 3C). In addition, the TF. RDN group had more *Bacteroidia* than the FF. RDN group (Fig. 3E).

Analysis of the gut microbiota composition at the order level

Figure 4A showed that *Oscillospirales* was the dominant bacteria in the F. NRDN group. The abundance of *Acidaminococcales* was increased in the F. RDN group. In the FF. RDN group, *Enterobacterales*, *Erysipelotrichales* and *Clostridiales* were enriched.

The abundance of *Lactobacillales* was higher in the NF. RDN (17%) and F. RDN groups (19%) than that in the FF. RDN (1%) and TF. RDN groups (4%). Additionally, *Bacteroidales* and *Clostridia_UCG−014* had similar trends among these four groups. Furthermore, *Enterobacterales* existed mainly in the F. RDN (9%) and FF. RDN (44%) groups, and only a few in the NF. RDN (0.5%) (Fig. 4B).

There were more *Bacteroidales* (Fig. 4C), *Rhodospirillales* (Fig. 4D), *Clostridia_UCG−014* (Fig. 4E), and *Acholeplasmatales* (Fig. 4F), and fewer *Monoglobales* (Fig. 4G) and *Enterobacterales* (Fig. 4H) in the NF. RDN group than in the F. RDN group.

Welch's t-test analysis showed that the NF. RDN group had more *Rhodospirillales* and fewer *Monoglobales* than the F. RDN group (Fig. 3B). Compared with the NF. RDN group, the FF. RDN group had fewer *Lachnospirales*, *Bacteroidales*, *Oscillospirales*, *Clostridia_UCG−014* and *RF39* (Fig. 3C). The FF. RDN group had fewer *Lachnospirales*, *Oscillospirales* and *Clostridia_UCG−014* than the F. RDN group (Fig. 3D). Similarly, the abundances of *Lachnospirales*, *Bacteroidales*, *Oscillospirales*, and *Clostridia_UCG−014* were lower in the FF. RDN group than in the TF. RDN group (Fig. 3E).

Analysis of the gut microbiota composition at the family level

The top 35 bacteria showed that *UCG-10* and *Butyricicoccaceae* were detected by major in the NF. RDN group and *Ruminococcaceae* was abundant in the F. NRDN group. The abundance of *Acidaminacoccaceae* was dominant in the F. RDN group. In addition, *Bacteroidales_RF16_group*, *Bacteroidaceae* and *Bifidobacteriaceae* were enriched in the TF. RDN group (Fig. 5A).

As for the top ten microbial communities (Fig. 5B), *Enterobacteriaceae* existed mainly in the F. RDN (9%), FF. RDN (44%) and TF. RDN (2%) groups. The relative abundance of *Lachnospiraceae* was 18% in the F. NRDN and F. RDN groups, 14% in the NF. RDN group, 2% in the FF. RDN group and 19% in the TF. RDN group. The F. RDN group had less *Prevotellaceae* (Fig. 5C) and other bacteria (Fig. 5F) and more *Monoglobaceae* (Fig. 5D) and *Enterobacteriaceae* (Fig. 5E) compared with the NF. RDN group.

(See figure on next page.)

Fig. 2 Composition of the gut microbiota at the phylum and class levels. **A** Heatmap of the abundant bacteria and (**B**) relative abundance distribution of the top 10 bacteria in the control, NF. RDN, F. NRDN, F. RDN, FF. RDN and TF. RDN groups at the phylum level. **C** Comparison of *Bacteroidota* and *Proteobacteria* (**D**) in the F. RDN and NF. RDN groups at the phylum level. **E** Heatmap of the top bacteria and (**F**) relative abundance distribution of the top 10 bacteria in the control, NF. RDN, F. NRDN, F. RDN, FF. RDN and TF. RDN groups at the class level. **G** Comparison of *Bacteroidia* and *Alphaproteobacteria* (**H**) in the F. RDN and NF. RDN groups at the class level. * $p < 0.05$, ** $p < 0.01$, *** $p < 0.001$. RDN, renal denervation

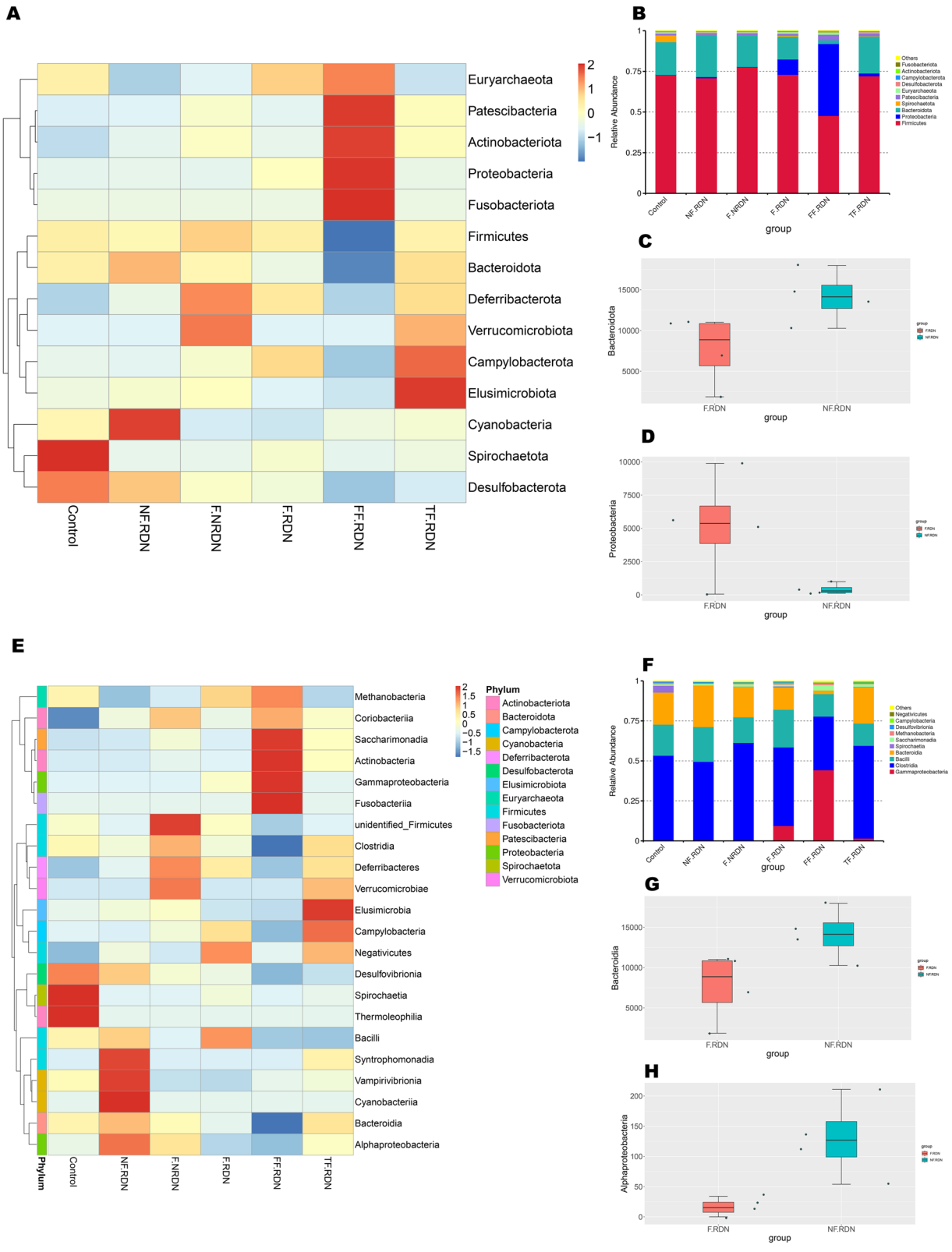

Fig. 2 (See legend on previous page.)

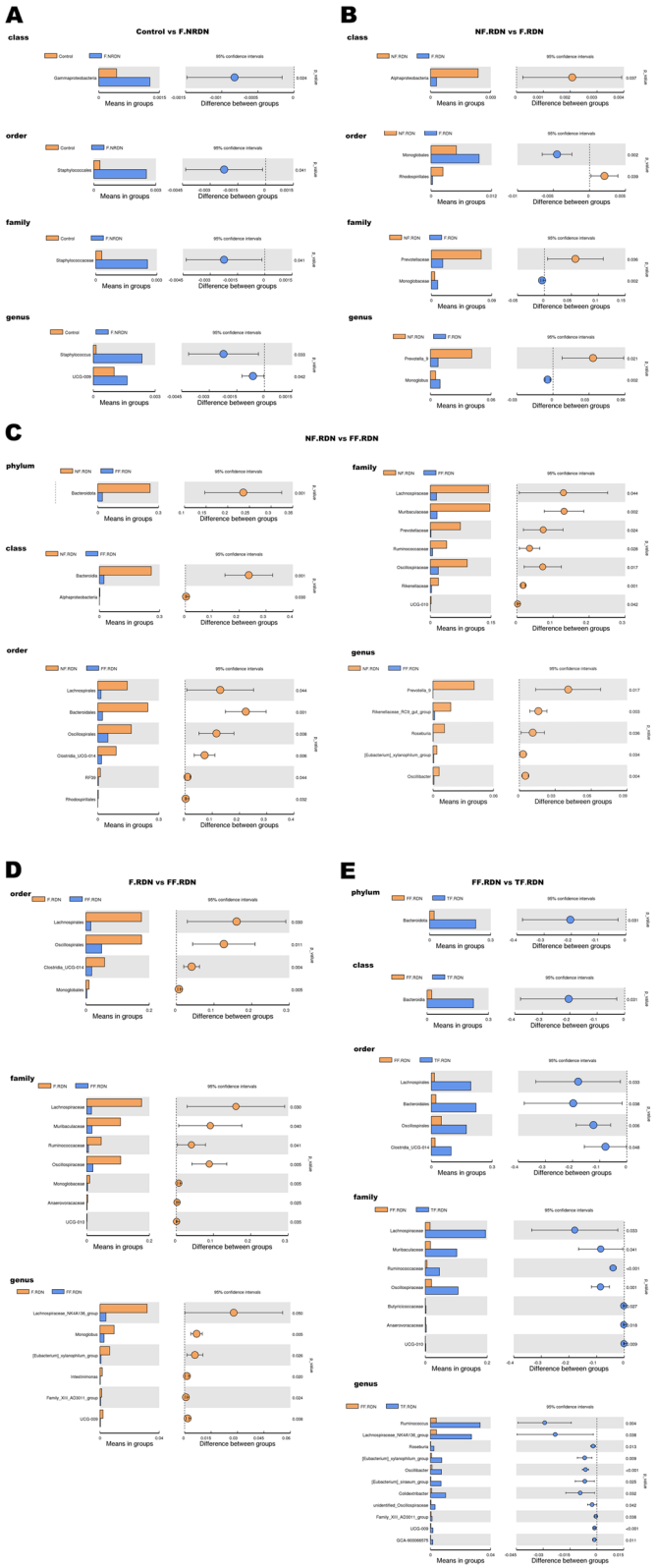

Fig. 3 T-test of differences in gut bacteria at different levels among different groups. **A** Distinct bacteria in the control and F. NRDN groups. **B** Distinct bacteria in the NF. RDN and F. RDN groups. **C** Distinct bacteria in the NF. RDN and FF. RDN groups. **D** Distinct bacteria in the F. RDN and FF. RDN groups. **E** Distinct bacteria in the FF. RDN and TF. RDN groups. $p < 0.05$ as per the test. RDN, renal denervation

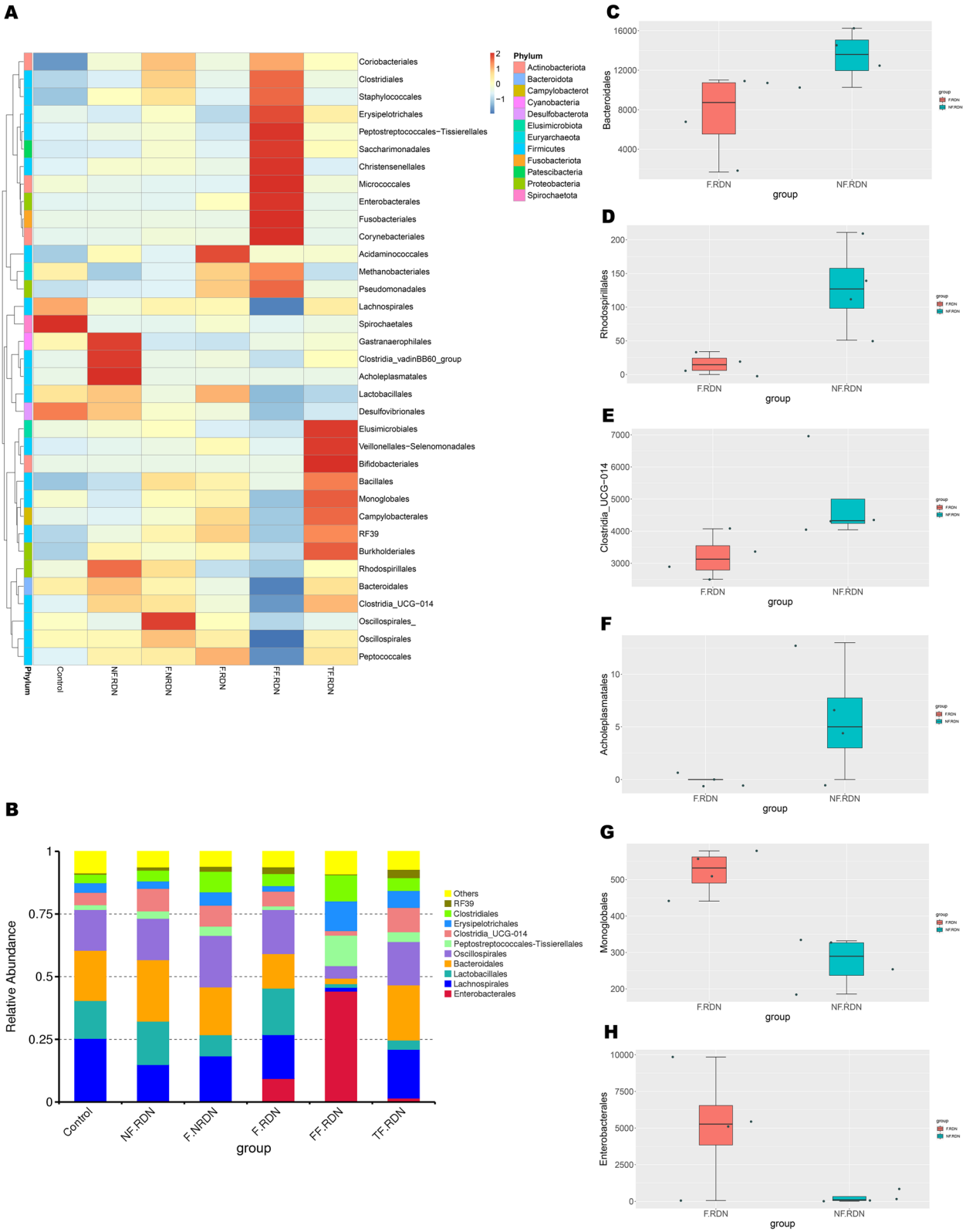

Fig. 4 Composition of the gut microbiota at the order level. **A** Heatmap of the top 35 bacteria and (**B**) relative abundance distribution of the top 10 bacteria in the control, NF. RDN, F. NRDN, F. RDN, FF. RDN and TF. RDN groups. **C** Comparison of *Bacteroidales,* **D** *Rhodospirillales*, **E** *Clostridia_UCG−014*, **F** *Acholeplasmatales*, **G** *Monoglobales* and (**H**) *Enterobacterales* in the F. RDN and NF. RDN groups. * $p < 0.05$, ** $p < 0.01$, *** $p < 0.001$. RDN, renal denervation

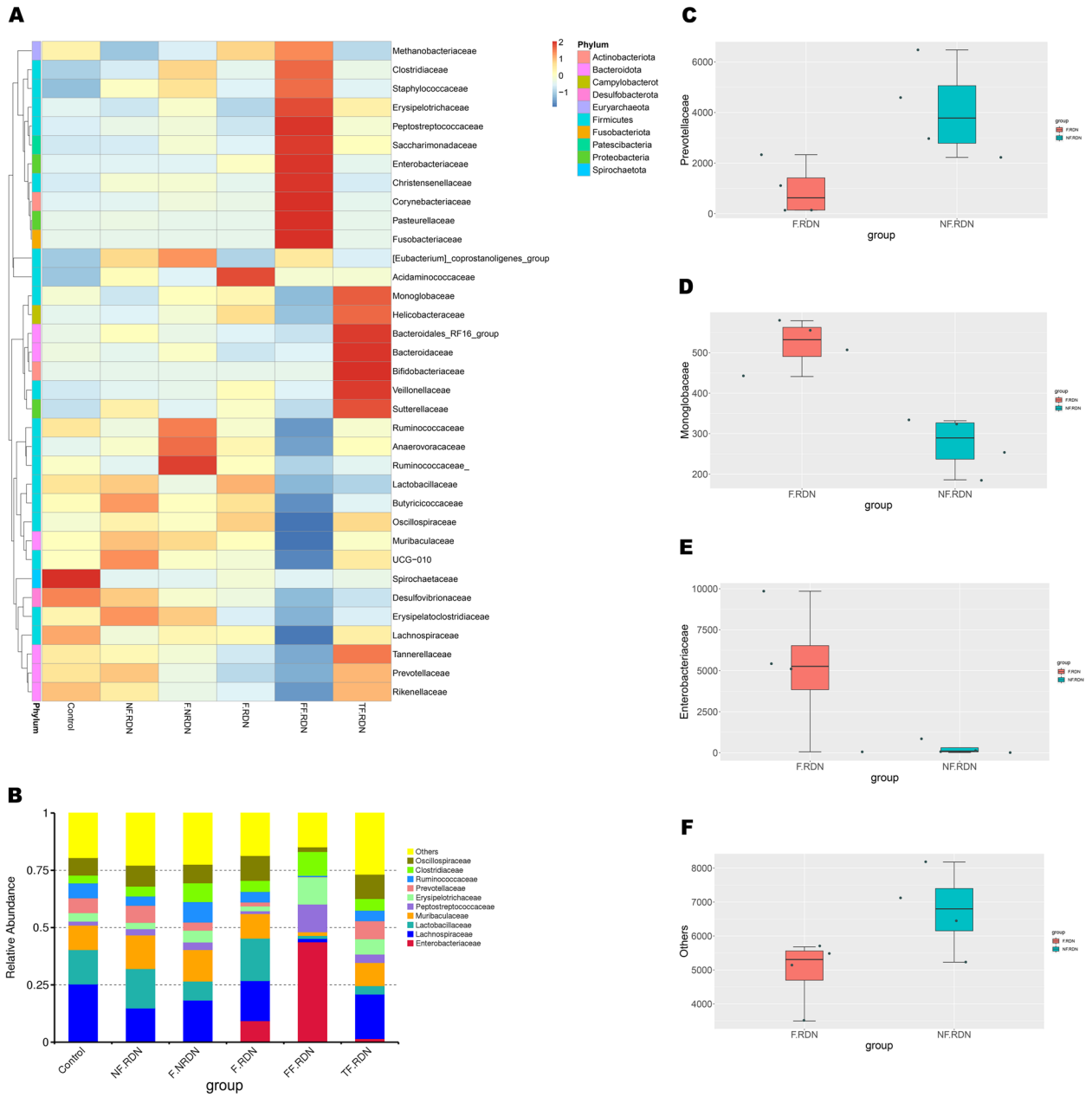

Fig. 5 Composition of the gut microbiota at the family level. **A** Heatmap of the top 35 bacteria and (**B**) relative abundance distribution of the top 10 bacteria in the control, NF. RDN, F. NRDN, F. RDN, FF. RDN and TF. RDN groups. **C** Comparison of *Prevotellaceae,* **D** *Monoglobaceae*, **E** *Enterobacteriaceae* and **F** others bacteria in the F. RDN and NF. RDN groups. * $p < 0.05$, ** $p < 0.01$, *** $p < 0.001$. RDN, renal denervation

Welch's t-test analysis showed that the F. RDN group had more *Monoglobaceae* and fewer *Prevotellaceae* than the NF. RDN group (Fig. 3B). Compared with the NF. RDN group, the FF. RDN group had fewer *Lachnospiraceae*, *Prevotellaceae*, *Ruminococcaceae* and *Oscillospiraceae* (Fig. 3C). Moreover, that the abundances of *Lachnospiraceae*, *Muribaculaceae*, *Ruminococcaceae*, *Oscillospiraceae* and *Monoglobaceae* were lower in the FF. RDN group than in the F. RDN group (Fig. 3D). However, the abundances of *Lachnospiraceae*, *Muribaculaceae*, *Ruminococcaceae*, *Oscillospiraceae* were increased in the TF. RDN group compared with the FF. RDN group (Fig. 3E).

Analysis of the gut microbiota composition at the genus level

Figure 6A showed that *Fournierella* and *Prevotella_9* were the dominant bacteria in the NF. RDN group and *Blautia* was predominant in the F. NRDN group. The abundances of *Lactobacillus*, *Oscillibacter* and *Roseburia* were greater in the F. RDN group than in the other groups.

The relative abundance of *Escherichia-Shigella* was 0.4% in the NF. RDN group, 9% in the F. RDN group, 44% in the FF. RDN group and 2% in the TF. RDN group (Fig. 6B). The F. RDN group had less *Prevotella_9* (Fig. 6C), *Anaeroplasma* (Fig. 6D) and more *Monoglobus* (Fig. 6E) and *UBA1819* (Fig. 6F) compared with the NF. RDN group.

The F. RDN group had more *Monoglobus* and fewer *Prevotella_9* than the NF. RDN group (Fig. 3B).

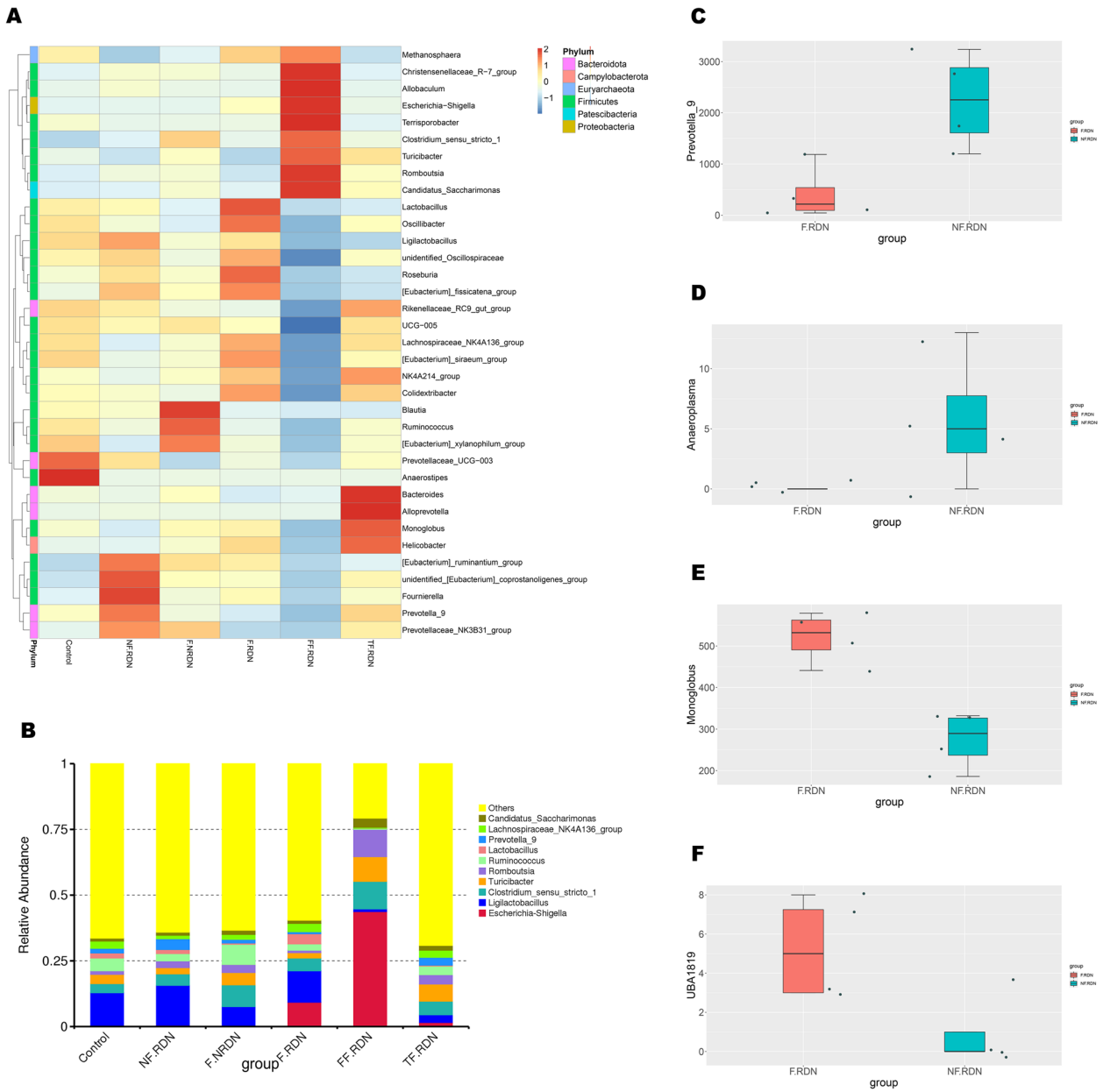

Fig. 6 Composition of the gut microbiota at the genus level. **A** Heatmap of the top 35 bacteria and (**B**) relative abundance distribution of the top 10 bacteria in the control, NF. RDN, F. NRDN, F. RDN, FF. RDN and TF. RDN groups. **C** Comparison of *Prevotella_9*, **D** *Anaeroplasma*, **E** *Monoglobus*, and (**F**) *UBA1819* in the F. RDN and NF. RDN groups. * $p < 0.05$, ** $p < 0.01$, *** $p < 0.001$. RDN, renal denervation

Prevotella-9, *Rikenellaceae_RC9_gut_group*, and *Oscillibacter* was decreased in the FF. RDN group compared with the NF. RDN group (Fig. 3C). In addition, the FF. RDN group also had fewer *Ruminococcus*, *Lachnospiraceae_NK4 A136_group*, *Roseburia* and *Oscillibacter* than the TF. RDN group (Fig. 3E).

Analysis of the gut microbiota composition at the species level

Figure 7A revealed the top 35 bacteria in abundance ranking at the species level. The top ten microbial communities showed that *swine_ fecal_bacterium_SD-Pec10* presented significant difference among the groups. Comparing with the F. RDN group (3%), the proportion of *swine_ fecal_bacterium_SD-Pec10* was higher in the FF. RDN group (7%). However, it was decreased in the TF, RDN group (2%) (Fig. 7B).

The abundances of *Bacteroides_sartorii* (Fig. 7C) and *Gram−negative_bacterium_cTPY−13* (Fig. 7D) were lower in the F. RDN group than in the NF. RDN group.

Tax4Fun function prediction

As shown in the heatmap of the abundance of functional categories (Fig. 8A), chromosome and associated proteins, peptidases, exosome and purine_metabolism were enriched in the NF. RDN group, while these functional pathways were decreased in the F. RDN group. Two-component_system, carbon_fixation_pathwaysin_prokaryotes, pyruvate_metabolism, and butanoate_metabolism were enriched in the FF. RDN group, and alanine, aspartate_and glutamate_metabolism, exosome were enriched in the TF. RDN group compared with the F. RDN group.

The petal diagram showed that the F. RDN group had 131 unique functional pathways and the FF. RDN group had 4 (Fig. 8B). As shown in Fig. 8C, the sample points between the F. RND and NF. RDN groups were closer than that between the FF. RDN and NF. RDN groups.

The Venn diagram revealed 148 unique functional pathways in the F. RDN group, 19 in the NF. RDN group and 26 in the control group (Fig. 8D). Additionally, there were 104 unique functional pathways in the F. RDN group and only 11 in the NF. RDN group when compared with these two groups separately (Fig. 8E).

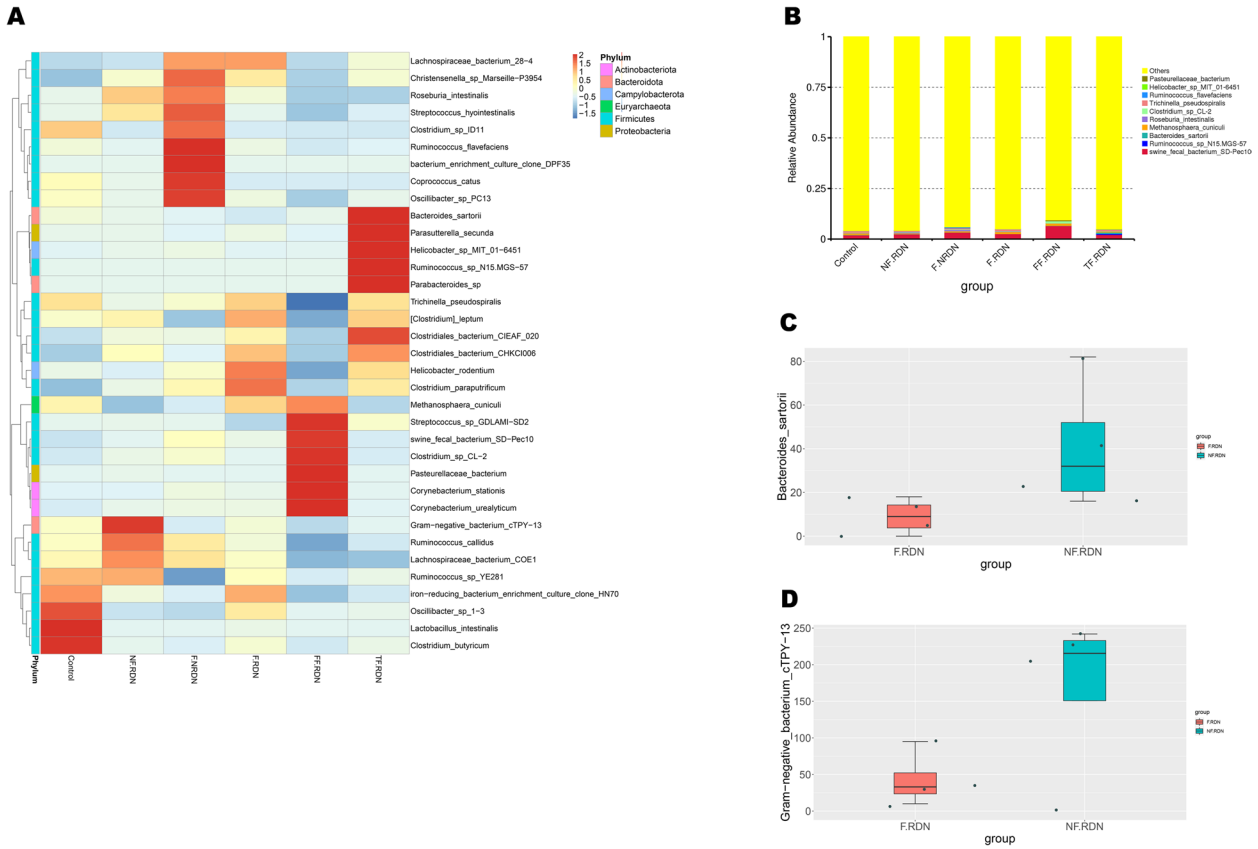

Fig. 7 Composition of gut microbiota at the species level. **A** Heatmap of the top 35 bacteria and (**B**) relative abundance distribution of the top 10 bacteria in the control, NF. RDN, F. NRDN, F. RDN, FF. RDN and TF. RDN groups. **C** Comparison of *Bacteroides_sartorii* and (**D**) *Gram−negative_bacterium_cTPY−13* in the F. RDN and NF. RDN groups. * $p < 0.05$, ** $p < 0.01$, *** $p < 0.001$. RDN, renal denervation

Fig. 8 Predictive functional profiling of microbial communities by Tax4 Fun analysis. **A** Heatmap based on Tax4 Fun functional annotations. **B** Petal diagrams and unique pathways among the intestinal bacterial communities of rats in the six groups. **C** Principal component analysis (PCA) plot showing the two principal components of the third-level KEGG functions. **D** Venn diagrams and unique pathways among the intestinal bacterial communities of rats in the control, NF. RDN and F. RDN groups, and (**E**) rats in the F. RDN and NF. RDN groups. **F** KEGG pathway annotation. **G** Comparison of enriched pathways based on KEGG (level 1), **H** KEGG (level 2) and (**I**) KEGG (level 3) between the NF. RDN and F. RDN groups. $p < 0.05$ as per the test. RDN, renal denervation; KEGG, Kyoto Encyclopedia of Genes and Genome

As shown in Fig. 8F, 49% of the genes were classified into seven KEGG functional categories. The categories associated with the greatest number of genes were environmental information processing (membrane transport 5.10%), genetic information processing (replication and repair 5.03%), and metabolism (carbohydrate metabolism 5.30%). The abundances of genes related to environmental information processing, genetic information processing, and metabolism were significantly different between the NF. RDN and F. RDN groups based on KEGG (level 1) (Fig. 8G). As shown in Fig. 8H, the KEGG (level 2) pathways for translation, glycan biosynthesis and metabolism, transport and catabolism, signaling molecules and interactions were decreased, while membrane transport, cell motility and signal transduction were increased in the F. RDN group compared with the NF. RDN group. The functional pathways with statistically significant differences between these two groups were also presented at the level 3 delicately (Fig. 8I).

Discussion

NAFLD is associated with gut microbiota dysbiosis and is critically involved in the development of heart failure. In the present study, the dissimilarity coefficients and the sample distances of the intestinal microbiome increased gradually with the presence and serious degree of NAFLD in HF rats induced by TAC. Compared with the NF. RDN group, the F. RDN group had fewer bacteria harmful to cardiac function, such as *Alphaproteobacteria, Bacteroidota* and *Prevotella-9*, and more bacteria beneficial to HF, such as *Monoglobaceae, Proteobacteria* and *Monoglobales*. This tendency also existed but was much less significant when compared the FF. RDN group with the NF. RDN group. However, there was no significant difference between the FF. RDN and TF. RDN groups. Predictive functional profiling of microbial communities showed that membrane transport, environmental and genetic information processing were significantly higher, and glycan biosynthesis and metabolism was significantly lower in the F. RDN group than in the NF. RDN

group. These findings indicated that NAFLD resulted in an increase in intestinal bacteria beneficial to HF and a decrease in intestinal bacteria harmful to HF in HF rats after RDN, which meant that the beneficial role of RDN in mitigating fecal microbiota aberrations in HF rats could be enhanced by NAFLD. However, these effects were significantly reduced with increasing severity of NAFLD.

NAFLD can cause gut microbiota dysbiosis [21]. Our results showed that HF rats with NAFLD had more *Gammaproteobacteria*, *Staphylococcaceae*, and *Staphylococcus* than control rats, suggesting that gut microbiota dysbiosis occurred not only in non-heart failure rats with NAFLD but also in heart failure rats with NAFLD, which existed diastolic dysfunction. *Gammaproteobacteria* was shown to promote the occurrence of fatty liver by producing endogenous ethanol [22] and deteriorate HF by producing trimethylamine [23, 24]. In addition, both *Staphylococcaceae* [25] and *Staphylococcus* [26] could accumulate in NAFLD and were related to significant myocardial dysfunction by mediating the inflammatory response through Toll-like receptor 2 [27]. Therefore, microbiota dysbiosis caused by NAFLD was critical to the severity and prognosis of HF, and NAFLD might influence the prognosis of HF by modulating gut bacteria and their products.

Our previous study showed that RDN improved gut microbiota aberrations [8]. In this study, significant alterations in the gut microbiota caused by NAFLD were observed in HF rats after RDN, suggesting that the influence of RDN on the intestinal microbiota in HF rats could be affected by the existence of NAFLD. The F. RDN group had fewer *Alphaproteobacteria, Bacteroidota* and *Prevotella-9*, which had been shown to be enriched in patients and experimental animals with cardiovascular disease [24] or NAFLD [28], and more *Monoglobaceae, Monoglobus, Proteobacteria* and *Monoglobales* than the NF. RDN group. *Alphaproteobacteria* and *Bacteroidota* could impact the prognosis of HF patients by influencing the production of trimethylamine N-oxide (TAMO) [24, 29], and *Prevotella_9* significantly increased in rats with spontaneously hypertensive heart failure and was associated with changes in cardiac structure and function [30] because of its pro-inflammatory role in chronic inflammation [31]. However, *Monoglobaceae, Monoglobus* and *Monoglobales* were shown to be able to stabilize the immune function of the gut by producing short-chain fatty acids (SCFAs) [32], which acted not only as energy substrates but also as anti-inflammatory factors and signaling molecules in the prevention and treatment of HF and other cardiovascular diseases [33, 34]. Furthermore, heatmap results also showed that *Oscillibacter, Roseburia* and *Helicobacter rodentium*, which were beneficial to cardiovascular disease [30, 35, 36], were enriched in the F. RDN group. These findings indicated that the existence of NAFLD could enhance themodulatory effect of RDN on the gut microbiota in HF rats by increasing beneficial bacteria and decreasing bacteria harmful to HF. Although NAFLD was associated with a higher risk of new-onset HF [37], left ventricular hypertrophy, systolic and diastolic dysfunction caused by activation of the renin–angiotensin and sympathetic nervous systems, insulin resistance, systemic inflammation and the gut microbiota [38, 39], all of which however could also be ameliorated by RDN [4, 40]. In terms of gut microbiota, HF rats with NAFLD could receive more significant benefits from RDN.

NASH evolves from NAFLD and is the more serious stage than NAFLD [41]. Whether the beneficial influence of NAFLD on the gut microbiota in HF rats after RDN could be further enhanced with the increase of severity of NAFLD is unclear. Our results showed that the FF.RDN group had fewer both *Bacteroidia, Prevotellaceae, Oscillospiraceae, Prevotella-9, Rikenellaceae_RC9_gut_group, Roseburia* and *Clostridia_UCG−014,* which were harmful to HF or cardiovascular system by up-regulating lipid proinflammatory metabolites [30, 42], and *Lachnospiraceae, Muribaculaceae, Ruminococcaceae, Oscillibacter* and *Lachnospirales,* which were beneficial to HF by increasing SCFA production, maintaining intestinal barrier function and inhibiting proinflammatory cytokines [43, 44], than the NF. RDN group. In contrast to the increases in beneficial gut microbiota and decreases in harmful bacteria in the F. RDN group, both the harmful and beneficial microbiota to HF were reduced in the FF. RDN group than in the NF. RDN group. This similar tendency was also observed between the FF. RDN and F. RDN groups. These findings indicated that the beneficial effect of NAFLD on enhancing the influence of RDN on modulating intestinal bacteria in HF was gradually reduced with the increase of the severity of NAFLD. Hepatic sympathetic overactivity is a key driver of hepatic steatosis. The decrease in liver sympathetic activity was related to improvements in liver triglyceride accumulation pathways including free fatty acid uptake and de novo lipogenesis [13]. Therefore, NAFLD itself could benefit from RDN by reducing hepatic sympathetic activity. However, sympathetic activity was not positively associated with the severity of NAFLD. Adori C et al. reported parallel signs of mild degeneration and axonal sprouting of sympathetic innervations in the early stages of NAFLD and a collapse of sympathetic nerves in steatohepatitis, and hepatic sympathetic nerve degeneration was correlated with the severity of NAFLD pathology [45]. This might be one of the possible reasons why

NASH did not gain more benefit from influencing the intestinal microbiota than NAFLD in HF rats after RDN.

Regarding the influence of NAFLD treatment on the intestinal microbiota in HF rats after RDN, no significant difference in the intestinal microbiota was observed between the treatment and nontreatment groups at from phylum to genus levels. Compared with the FF. NRDN group, there was an increase in both beneficial (such as *Lachnospiraceae, Muribaculaceae* and *Ruminococcaceae*) and harmful bacteria (such as *Bacteroidia, Oscillospiraceae* and *Roseburia*) to HF in the TF. RDN group. These findings indicated that NAFLD treatment did not further increase the beneficial roles of RDN in ameliorating aberrations of the gut microbiota further in HF rats with NAFLD, although NAFLD was detrimental to HF. The beneficial effect of RDN on the intestinal microbiota might be greater than that of treatment for NAFLD in HF rats with NAFLD.

In addition to microbial community composition, predictive functional analysis showed that many bacterial genes involved in glycan biosynthesis and metabolism, membrane transport and genetic information processing and other related pathways were significantly different between the F. RDN and NF. RDN groups. Glycan biosynthesis and metabolism was related to HF by modulating SCFA metabolism [30, 46]. Membrane transport was also associated with HF, of which sodium-dependent glucose transporters were their important members [47]. Therefore, NAFLD could play a genetic modulatory role by reducing pathogenic bacteria genes and increasing beneficial bacterial genes to HF in HF rats after RDN, which might help to partly explain the mechanism of the influence of NAFLD on the modulatory role of RDN on the intestinal microbiota.

Several limitations should be discussed. First, some critical bacterial products, such as TMAO and SCFAs, were not detected in this study. Second, intestinal functions were not explored because metabolites produced by the intestinal flora associated with HF were mainly absorbed in intestine, and their levels in the blood might be affected by the functional state of intestine. Finally, the effect of UDCA on the treatment of NAFLD in rats with HF was not assessed, so the degree to which UDCA ameliorated NAFLD was unknown.

Conclusions

NAFLD could lead to an increase in beneficial bacteria and a decrease in bacteria harmful to cardiac function in HF rats after RDN, but this useful alteration of the gut microbiota decreased with the severity of NAFLD, suggesting that mild and moderate NAFLD might enhance the ability of RDN to improve gut microbiota aberrations in HF rats.

Abbreviations

RDN	Renal denervation
NAFLD	Non-alcoholic fatty liver disease
HF	Heart failure
NASH	Non-alcoholic steatohepatitis
TAC	Transverse aortic constriction
UDCA	Ursodeoxycholic acid
ANOSIM	Analysis of similarity
AMOVA	Analysis of molecular variance
LEfSe	Linear discriminant analysis effect size
TAMO	Trimethylamine N-oxide
SCFAs	Short-chain fatty acids

Supplementary Information

The online version contains supplementary material available at https://doi.org/10.1186/s12866-025-04027-y.

Supplementary Material 1: Supplementary Figure 1. The animal grouping and timeline of the experimental protocol.

Supplementary Material 2: Supplemental Figure S2. Body weight and liver index of rats in the control, F.RDN, and FF.RDN groups. (A) The trend of body weight changes in each group of rats. (B) Liver index of rats in each group. * vs Control, $P< 0.05$; # vs NAFLD, $P < 0.05$.

Supplementary Material 3: Supplemental Figure S3. Representative micrographs of livers hematoxylin-eosin (HE) staining of the control, NF.RDN, F.NRDN, F.RDN, FF.RDN, TF.RDN groups. Long arrow: venae centrales hepatis, short arrow: steatosis, triangle: ballooning. RDN, renal denervation.

Supplementary Material 4: Supplemental Figure S4. Representative micrographs of oil red O staining, masson staining of liver and parameters of echocardiography in different groups. (A) Oil red O staining of different groups (40×). (B) Quantitative analysis of relative fat content in the livers of different groups. (C) Masson staining of different groups (40×). (D) Quantitative analysis of relative fiber content in the livers of various groups. (E) Comparison of left ventricular ejection fraction. (F) Comparison of left ventricular end-systolic diameter. (G) Comparison of left ventricular end-diastolic diameter. (H) Lung to body weight index. (I) The ratio of the E and A peak flow rate. * $p< 0.05$, ** $p < 0.01$. RDN, renal denervation.

Authors' contributions

PAC contributed to the design of the experiments. FYC, ZQG, YFC and SL performed the experiments. FYC, ZQG and PAC wrote the main manuscript text and FYC, ZQG and PAC prepared figures 1-8. All authors reviewed and approved the final manuscript.

Funding

This work was supported by National Natural Science Foundation of China [grant number 81770398]; and Science and Technology Planning Project Foundation of Guangzhou [grant number 202201020283].

Data availability

Data is provided within the manuscript or supplementary information files. All data supporting this study's findings are available at https://www.ncbi.nlm.nih.gov/sra/PRJNA1083302.

Declarations

Ethics approval and consent to participate

The research animals were treated and manipulated following the ARRIVE guidelines (https://arriveguidelines.org). The investigation was approved by the institutional ethics committee of Guangzhou First People's Hospital.

Consent for publication

Not applicable.

Competing interests

The authors declare no competing interests.

Received: 23 February 2024 Accepted: 6 May 2025
Published online: 21 May 2025

References

1. Baman JR, Ahmad FS. Heart Failure. JAMA. 2020;324:1015.
2. Drapala A, Szudzik M, Chabowski D, Mogilnicka I, Jaworska K, Kraszewska K, et al. Heart failure disturbs gut-blood barrier and increases plasma trimethylamine, a toxic bacterial metabolite. Int J Mol Sci. 2020;21:6161.
3. Sandek A, Bauditz J, Swidsinski A, Buhner S, Weber-Eibel J, von Haehling S, et al. Altered intestinal function in patients with chronic heart failure. J Am Coll Cardiol. 2007;50:1561–9.
4. Sharp TE 3rd, Lefer DJ. Renal denervation to treat heart failure. Annu Rev Physiol. 2021;83:39–58.
5. Sharp TE 3rd, Polhemus DJ, Li Z, Spaletra P, Jenkins JS, Reilly JP, et al. Renal denervation prevents heart failure progression via inhibition of the renin-angiotensin system. J Am Coll Cardiol. 2018;72:2609–21.
6. Zheng H, Katsurada K, Liu X, Knuepfer MM, Patel KP. Specific afferent renal denervation prevents reduction in neuronal nitric oxide synthase within the paraventricular nucleus in rats with chronic heart failure. Hypertension. 2018;72:667–75.
7. Lu D, Wang J, Zhang H, Shan Q, Zhou B. Renal denervation improves chronic intermittent hypoxia induced hypertension and cardiac fibrosis and balances gut microbiota. Life Sci. 2020;262:118500.
8. Guo Z, Chen Y, Chen S, Liu C, Li S, Chen P. Renal denervation mitigated fecal microbiota aberrations in rats with chronic heart failure. Evid Based Complement Alternat Med. 2021;2021:1697004.
9. Guo Z, Chen F, Chen Y, Liu C, Li S, Chen P. Inhibiting intestinal Kruppel-Like factor 5 impairs the beneficial role of renal denervation in gut microbiota in rats with heart failure. Microbiol Spectr. 2022;10:e0218322.
10. Jonas W, Schurmann A. Genetic and epigenetic factors determining NAFLD risk. Mol Metab. 2021;50:101111.
11. Simon TG, Bamira DG, Chung RT, Weiner RB, Corey KE. Nonalcoholic steatohepatitis is associated with cardiac remodeling and dysfunction. Obesity (Silver Spring). 2017;25:1313–6.
12. Fotbolcu H, Yakar T, Duman D, Karaahmet T, Tigen K, Cevik C, et al. Impairment of the left ventricular systolic and diastolic function in patients with non-alcoholic fatty liver disease. Cardiol J. 2010;17:457–63.
13. Hurr C, Simonyan H, Morgan DA, Rahmouni K, Young CN. Liver sympathetic denervationreverses obesity-induced hepatic steatosis. J Physiol. 2019;597(17):4565–80. https://doi.org/10.1113/JP277994. Epub 2019 Jul 26. PMID: 31278754; PMCID: PMC6716997.
14. Aron-Wisnewsky J, Vigliotti C, Witjes J, Le P, Holleboom AG, Verheij J, et al. Gut microbiota and human NAFLD: disentangling microbial signatures from metabolic disorders. Nat Rev Gastroenterol Hepatol. 2020;17:279–97.
15. Khamphaya T, Chukijrungroat N, Saengsirisuwan V, Mitchell-Richards KA, Robert ME, Mennone A, et al. Nonalcoholic fatty liver disease impairs expression of the type II inositol 1,4,5-trisphosphate receptor. Hepatology. 2018;67:560–74.
16. Van Herck MA, Vonghia L, Francque SM. Animal models of nonalcoholic fatty liver disease-a starter's guide. Nutrients. 2017;9:1072.
17. Tetri LH, Basaranoglu M, Brunt EM, Yerian LM, Neuschwander-Tetri BA. Severe NAFLD with hepatic necroinflammatory changes in mice fed trans fats and a high-fructose corn syrup equivalent. Am J Physiol Gastrointest Liver Physiol. 2008;295:G987-95.
18. Chen Y, Guo Z, Li S, Liu Z, Chen P. Spermidine affects cardiac function in heart failure mice by influencing the gut microbiota and cardiac galectin-3. Front Cardiovasc Med. 2021;8:765591.
19. Kouakou JL, Gonedelé-Bi S, Assamoi JB, AssanvoN'Guetta SP. Optimization of the Cetyltrimethylammonium bromide (CTAB) DNA extraction protocol using forest elephant dung samples. MethodsX. 2022;9:101867.
20. Wang Z, Li S, Wang R, Guo L, Xu D, Zhang T, et al. The protective effects of the β3 adrenergic receptor agonist BRL37344 against liver steatosis and inflammation in a rat model of high-fat diet-induced nonalcoholic fatty liver disease (NAFLD). Mol Med. 2020;26:54.
21. Zhao ZH, Xin FZ, Xue Y, Hu Z, Han Y, Ma F, et al. Indole-3-propionic acid inhibits gut dysbiosis and endotoxin leakage to attenuate steatohepatitis in rats. Exp Mol Med. 2019;51:1–14.
22. Michail S, Lin M, Frey MR, Fanter R, Paliy O, Hilbush B, et al. Altered gut microbial energy and metabolism in children with non-alcoholic fatty liver disease. FEMS Microbiol Ecol. 2015;91:1–9.
23. Rath S, Heidrich B, Pieper DH, Vital M. Uncovering the trimethylamine-producing bacteria of the human gut microbiota. Microbiome. 2017;5:54.
24. Zhao J, Zhang Q, Cheng W, Dai Q, Wei Z, Guo M, et al. Heart-gut microbiota communication determines the severity of cardiac injury after myocardial ischaemia/reperfusion. Cardiovasc Res. 2023;119:1390–402.
25. Pan X, Kaminga AC, Liu A, Wen SW, Luo M, Luo J. Gut microbiota, glucose, lipid, and water-electrolyte metabolism in children with nonalcoholic fatty liver disease. Front Cell Infect Microbiol. 2021;11:683743.
26. Tsai HY, Shih YY, Yeh YT, Huang CH, Liao CA, Hu CY, et al. Pterostilbene and its derivative 3'-hydroxypterostilbene ameliorated nonalcoholic fatty liver disease through synergistic modulation of the gut microbiota and SIRT1/AMPK signaling pathway. J Agric Food Chem. 2022;70:4966–80.
27. Knuefermann P, Sakata Y, Baker JS, Huang CH, Sekiguchi K, Hardarson HS, et al. Toll-like receptor 2 mediates Staphylococcus aureus-induced myocardial dysfunction and cytokine production in the heart. Circulation. 2004;110:3693–8.
28. Sookoian S, Salatino A, Castano GO, Landa MS, Fijalkowky C, Garaycoechea M, et al. Intrahepatic bacterial metataxonomic signature in non-alcoholic fatty liver disease. Gut. 2020;69:1483–91.
29. Bin-Jumah MN, Gilani SJ, Hosawi S, Al-Abbasi FA, Zeyadi M, Imam SS, et al. Pathobiological relationship of excessive dietary intake of choline/L-carnitine: a TMAO precursor-associated aggravation in heart failure in sarcopenic patients. Nutrients. 2021;13:3453.
30. Gutierrez-Calabres E, Ortega-Hernandez A, Modrego J, Gomez-Gordo R, Caro-Vadillo A, Rodriguez-Bobada C, et al. Gut microbiota profile identifies transition from compensated cardiac hypertrophy to heart failure in hypertensive rats. Hypertension. 2020;76:1545–54.
31. Larsen JM. The immune response to prevotella bacteria in chronic inflammatory disease. Immunology. 2017;151:363–74.
32. Wu X, Huang X, Ma W, Li M, Wen J, Chen C, et al. Bioactive polysaccharides promote gut immunity via different ways. Food Funct. 2023;14:1387–400.
33. Challa AA, Lewandowski ED. Short-chain carbon sources: exploiting pleiotropic effects for heart failure therapy. JACC Basic Transl Sci. 2022;7:730–42.
34. Hu T, Wu Q, Yao Q, Jiang K, Yu J, Tang Q. Short-chain fatty acid metabolism and multiple effects on cardiovascular diseases. Ageing Res Rev. 2022;81:101706.
35. Seo J, Matthewman L, Xia D, Wilshaw J, Chang YM, Connolly DJ. The gut microbiome in dogs with congestive heart failure: a pilot study. Sci Rep. 2020;10:13777.
36. Warme J, Sundqvist MO, Hjort M, Agewall S, Collste O, Ekenback C, et al. Helicobacter pylori and pro-Inflammatory protein biomarkers in myocardial infarction with and without obstructive coronary artery disease. Int J Mol Sci. 2023;24:14143.
37. Mantovani A, Petracca G, Csermely A, Beatrice G, Bonapace S, Rossi A, et al. Non-alcoholic fatty liver disease and risk of new-onset heart failure: an updated meta-analysis of about 11 million individuals. Gut. 2022:gutjnl-2022-327672.
38. Zhou J, Bai L, Zhang XJ, Li H, Cai J. Nonalcoholic fatty liver disease and cardiac remodeling risk: pathophysiological mechanisms and clinical implications. Hepatology. 2021;74:2839–47.
39. Petta S, Argano C, Colomba D, Camma C, Di Marco V, Cabibi D, et al. Epicardial fat, cardiac geometry and cardiac function in patients with non-alcoholic fatty liver disease: association with the severity of liver disease. J Hepatol. 2015;62:928–33.
40. Rey-Garcia J, Townsend RR. Renal denervation: a review. Am J Kidney Dis. 2022;80:527–35.
41. Barrow F, Khan S, Wang H, Revelo XS. The emerging role of B cells in the pathogenesis of NAFLD. Hepatology. 2021;74:2277–86.
42. Brandsma E, Kloosterhuis NJ, Koster M, Dekker DC, Gijbels MJJ, van der Velden S, et al. A proinflammatory gut microbiota increases systemic inflammation and accelerates atherosclerosis. Circ Res. 2019;124:94–100.
43. Baxter NT, Schmidt AW, Venkataraman A, Kim KS, Waldron C, Schmidt TM. Dynamics of human gut microbiota and short-chain fatty acids in

response to dietary interventions with three fermentable fibers. mBio. 2019;10:e02566-18.
44. He J, Guo K, Chen Q, Wang Y, Jirimutu. Camel milk modulates the gut microbiota and has anti-inflammatory effects in a mouse model of colitis. J Dairy Sci. 2022;105:3782–93.
45. Adori C, Daraio T, Kuiper R, Barde S, Horvathova L, Yoshitake T, et al. Disorganization and degeneration of liver sympathetic innervations in nonalcoholic fatty liver disease revealed by 3D imaging. Sci Adv. 2021;7:eabg733.
46. Chen T, Zhang Y, Zhang Y, Shan C, Zhang Y, Fang K, et al. Relationships between gut microbiota, plasma glucose and gestational diabetes mellitus. J Diabetes Investig. 2021;12:641–50.
47. Khan F, Elgeti M, Grandfield S, Paz A, Naughton FB, Marcoline FV, et al. Membrane potential accelerates sugar uptake by stabilizing the outward facing conformation of the Na/glucose symporter vSGLT. Nat Commun. 2023;14:7511.

Publisher's Note